QUANTITATIVE MODELING OF SOUND SOURCES AROUND CIVIL AIRCRAFT ON FINAL APPROACH

Takehisa Takaishi[1], Tomohiro Kobayashi[2], Takayuki Kato[3],
Keiji Shimoda[3], and Takatoshi Yokota[2]

[1]Japan Aerospace Exploration Agency
6-13-1 Osawa, Mitaka, Tokyo 181-0015, Japan
[2]Kobayasi Institute of Physical Research
[3]IHI Aerospace Engineering

ABSTRACT

Precise sound source modelling is needed to better evaluate the acoustic influences of landing gear and high-lift devices, to estimate the effectiveness of noise reduction technologies applied to them, and to investigate when they should be extended for landing. To model sound sources of civil aircraft, a 30 m-diameter microphone array was set up under the approach path to runway 16L at Narita International Airport in Japan, and a total of 186 civil aircraft flight passes on final approach with 25 aircraft types and 33 engine types were measured over three days. Beamforming in the time domain was applied, and acoustical maps were obtained at five emission angles. In case of the latest aircraft types with high-bypass turbofan engines, such as the Boeing 787, the nose and main landing gears were found to be the dominant noise sources. To model the sound power levels and directivities of each sound source, acoustical maps were integrated over 13 partial regions around the aircraft. The CLEAN algorithm applied to the limited regions of interest gave good estimations, and the predicted time history of sound pressure level on the ground agreed very well with measured values. In case of the B787-8, airframe noise was found to be responsible for 3/4 of L_{AE}.

1   INTRODUCTION

People living around airports have been exposed to significant aircraft noise for many years. In early jet era, turbojet engines were responsible for much of the noise, but engine noise has reduced substantially since the development of high-bypass ratio turbofan engines. Correspondingly, the proportion of aircraft noise generated by the airframe has increased, particularly by high lift-devices and the landing gear during final approach. The Japan Aerospace Exploration Agency (JAXA) launched the FQUROH (Flight demonstration of Quiet Technology to Reduce Noise from High-lift configurations) project in 2015 to verify

through flight demonstration the feasibility of practical airframe noise reduction concepts such as modified high-lift devices and landing gear. In its second flight demonstration conducted in 2017, the overall sound pressure levels (SPLs) around the main landing gear and flaps were reduced by 4.4 dB and 3.5 dB, respectively [1]. An acoustic phased array with 195 microphones was used to evaluate the effectiveness of the noise reduction devices.

As another application of this advanced noise measurement capability, detailed sound source properties, including the precise position and frequency characteristics of emitters on and around an aircraft, can be used to construct an acoustic model of an aircraft that can be used to predict aircraft noise around airports. There are two major types of aircraft noise prediction model. One is the segmentation method used by tools such as the FAA's AEDT and EUROCONTROL's STAPES. These represent an aircraft as a point source of sound and are widely used for airport noise control because they can provide noise contours around airports in short computation time. However, they cannot evaluate the contributions of each discrete sound source. The other is the detailed simulation model, used in tools such as NASA's ANNOP. This consists of precise models for each component and is widely used in aircraft design (especially for type certification), but it is often difficult to obtain the non-disclosed technical information. We therefore decided to make a noise prediction model from acoustic maps obtained by a microphone array, and demonstrated its capability using measured data of JAXA's test aircraft as an example [2, 3].

In May 2019, sound sources around civil aircraft on final approach were measured by a 30 m-diameter microphone array deployed under the approach path to runway 16L of Narita International Airport. This paper presents the resulting aircraft acoustic maps and discusses improvements to postprocessing to obtain better agreement with ground SPL measurements.

2   FLYOVER TEST

2.1   Array setup

Fig. 1. Microphone array being deployed under the flight path.

Figure 1 show the 30 m-diameter microphone array which was deployed under the flight path to runway 16L at Narita International Airport. In the previous flyover tests conducted at Noto Airport, the microphone array was mounted on a 35 x 35 m square temporary platform built beside the airport's runway [1, 2], but it cost about 13 million yen (110 thousand Euro) and took a lot of manpower to build the platform and install the microphones. To reduce the effort

to construct the Narita airport array, each microphone was mounted on a 200 mm-diameter circular plate modeled on a microphone holder using a silicone mold. These could be quickly placed directly on the ground as shown in Fig. 1. To further reduce the array set-up time and to confirm various technical issues, the number of microphones was also reduced. While previous tests had used 195 microphones distributed in 13 radial arms of 15 microphones each arranged in a geometric progression of intervals, the Narita airport array used 90 quarter-inch microphones in 6 radial arms of 15 microphones. Figure 2 compares the theoretical performances of these microphone arrays. The half-power beam width is defined as the angle between the half power (-3 db) points of the main lobe, and main lobe to sidelobe ratio is defined as the ratio of the power of the main lobe to the power of the strongest sidelobe. The half-power beam width (resolution) is the same for both arrays, but the main lobe to sidelobe ratio decreases as the number of microphones is reduced.
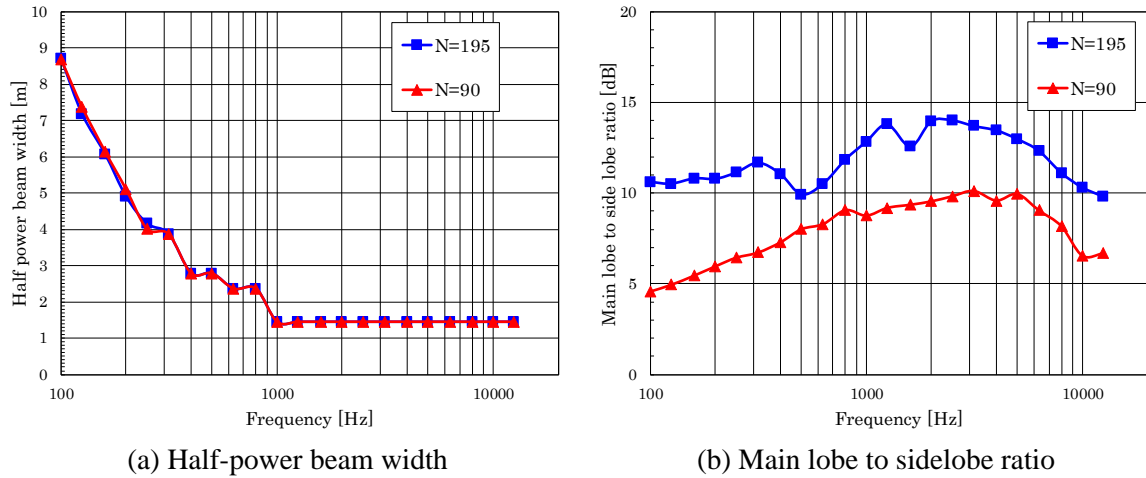

(a) Half-power beam width   (b) Main lobe to sidelobe ratio

Fig. 2. Comparison of array performances with different number of microphones.

2.2 Flight path estimation

It is difficult to obtain aircraft tracking data sufficiently accurate to calculate the propagation of sounds from noise sources to each microphone at each moment in time. The test site was located under the extended runway centerline 1,210 m from the runway threshold, and all aircraft descended at a glideslope angle of 3°. Line sensor cameras with light-sensing arrays oriented perpendicularly to the flight direction were used to calculate ground speed, altitude, and lateral deviation from the extended runway centerline when the aircraft passed directly above the microphone array. The flight path was then reconstructed assuming that the airplane was flying on the glideslope at a constant linear velocity before and after the measurement point.

2.3 Analytical method

Beamforming in the time domain was applied to calculate acoustic maps around each aircraft. Suppose that a moving point source at position $\boldsymbol{\xi}(\tau)$ radiates a sound signal of strength $\sigma(\tau)$ at time τ, and that the radiated sound is received by the nth microphone in an array at position $\boldsymbol{x}_n$ at time t_n. The received acoustic pressure $\chi_n(t_n)$ is given in the form

$$\chi_n(t_n) = \frac{\sigma(\tau)}{4\pi\left\{\left\|\mathbf{x}_n - \boldsymbol{\xi}(\tau)\right\| - \boldsymbol{\xi}'(\tau)\cdot\left(\mathbf{x}_n - \boldsymbol{\xi}(\tau)\right)/c\right\}} \tag{1}$$

3

[4], and the retarded time τ is the solution of the equation

$$t_n - \tau = \|\mathbf{x}_n - \boldsymbol{\xi}(\tau)\| / c \tag{2}$$

where c is the speed of sound. Equation (1) is based on the mathematical transform from a moving reference frame to a static coordinate system. The denominator includes amplifier modification due to the Doppler effect, and is simplified as $4\pi R(1 - Mcos\theta)$ where $R \equiv \|\mathbf{x}_n - \boldsymbol{\xi}(\tau)\|$, $M \equiv \|\boldsymbol{\xi}'(\tau)\|/c$, and θ is the emission angle between the path of the sound and the path of the moving point source at time τ. The acoustic pressure received by microphones also includes a frequency shift due to Doppler effect, and this will be corrected when the time history of $\sigma(\tau)$ in the moving coordinate system is resampled (de-Dopplerized [5]) by Eqn. (1). For each focused moving point $\boldsymbol{\xi}_b$ in the source region, the expression of conventional Delay and Sum beamforming in the time domain is

$$b(\boldsymbol{\xi}_b, \tau) = \sum_{n=1}^{N} \frac{1}{N} \sigma_n(\boldsymbol{\xi}_b, \tau) \tag{3}$$

where N is the total number of microphones in the array. Transforming Eqn. (3) into the frequency domain yields

$$\tilde{b}(\boldsymbol{\xi}_b, \omega) = \sum_{n=1}^{N} \frac{1}{N} \tilde{\sigma}_n(\boldsymbol{\xi}_b, \omega) \tag{4}$$

where ω is angular frequency.

The source power spectrum $A(\omega)$ is calculated as

$$A(\omega) = \frac{1}{2} \sum_{n=1}^{N} \sum_{m=1}^{N} w_n(\omega) w_m(\omega) \tilde{\sigma}_n(\boldsymbol{\xi}_b, \omega) \tilde{\sigma}_m^*(\boldsymbol{\xi}_b, \omega) \tag{5}$$

in which the asterisk denotes complex conjugation. A frequency-dependent weighting factor $w_n(\omega)$ should be $1/N$ if the contributions of all of microphones in the array are equal. In the current study, the weight factor was customized as

$$w_n(\omega) = r_n^{(2\times(200\times2\pi/\omega)^{1/2})} \times \frac{1}{2} \left\{ 1 - \mathrm{Erf}\left[2 \times \left(\frac{r_n}{R_{effect}(\omega)} - 1 \right) \right] \right\} \tag{6}$$

$$R_{effect}(\omega) = 10000 \times 3 \times 2\pi / \omega \tag{7}$$

where r_n is the distance from the nth microphone to the array center, and Erf abbreviates an error function. Auto-correlations of $A(\omega)$ were removed to eliminate self-noise caused by natural wind.

$$A(\omega) = \frac{1}{2} \left| \tilde{b}(\boldsymbol{\xi}_b, \omega) \right|^2 = \frac{1}{2} \sum_{n=1}^{N} \sum_{\substack{m=1 \\ m\neq n}}^{N} w_n(\omega) w_m(\omega) \tilde{\sigma}_n(\boldsymbol{\xi}_b, \omega) \tilde{\sigma}_m^*(\boldsymbol{\xi}_b, \omega) \tag{8}$$

Since the microphones were installed on the ground, the amplitudes of incident sound waves would be doubled by reflection waves, so $20\log_{10} 2 = 6.0$ dB was subtracted from beamforming results. Air absorption during propagation was corrected based on ISO 9613-1:1993. Displacement due to convection by wind was also corrected. Meteorological observation data recorded by a weather station beside the microphone array were used for these corrections.

Acoustic maps at different emission angles were calculated to provide the directivity of sound radiated from each sound source. Figure 3 illustrates the geometry of sound emission during a microphone array flyover. Emission angle is defined as the angle between the flight path (=the 3° glideslope assumed in section 2.2) and the path of the sound radiated toward the reference microphone at the array center. Discrete Fourier Transform (DFT) analysis was applied when the aircraft was within ±10 m of the position determined by the emission angle,

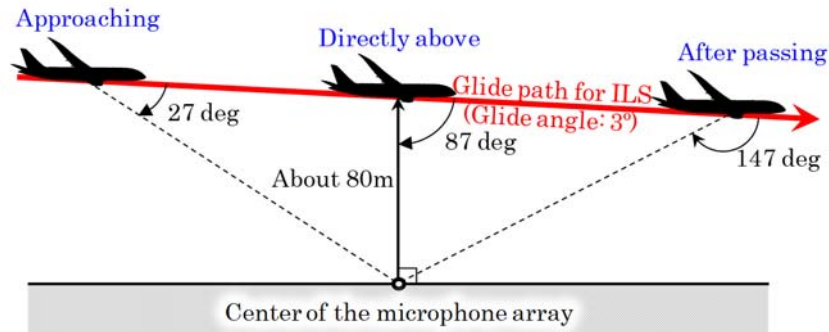and results from about thirty DFT blocks (depending on the ground speed) were power-averaged.

Fig. 3. Geometry of sound emission during flyover.

2.4   Overview of measurement

The flyover test was conducted on three days in May 2019 when a light wind was coming from the south and aircraft landing on runway 16L flew over the test site located under the extended runway centerline north of the runway threshold. A total of 186 flight passes on final approach with 25 aircraft types and 33 engine types were measured. Table 1 summarizes types of aircraft and engine measured.

Table 1. Measured aircraft and engine types.

Aircraft	Length [m]	Wingspan [m]	Engine	Number measured
B737-800 with winglets	39.47	35.79	CFM56-7B	29
B747-400	70.67	64.92	CF6-80C2	1
B767-300	54.94	47.57	CF6-80C2	11
B767-300 with winglets	54.94	50.88	CF6-80C2	15
			PW4060	2
B777-200	63.73	60.93	GE90	3
			Trent 800	3
B777-300	73.86	60.93	Trent 800	2
B777-300ER	73.86	64.80	GE90-115B	6
B777 Freighter	63.73	64.80	GE90-115B	2
B787-8	56.72	60.12	Genx-1B70	18
			Trent 1000	11
B787-9	62.81	60.12	Genx-1B	4
			Trent 1000	4
A319-100	33.84	34.10	CFM56-5B	2
A320-200	37.57	34.10	CFM56-5B	5
			V2527-A5	7
A320-200 with Sharklet	37.57	35.80	CFM56-5B	7
			V2527-A5	19
A320-200N with Sharklet	37.57	35.80	PW1127G	3
A321-200	44.51	34.10	V2533-A5	2

A321-200 with Sharklet	44.51	35.80	CFM56-5B	2
			V2533-A5	7
A330-200	58.82	60.30	Trent 772	1
A330-300	63.67	60.30	CF6-80EB	1
			Trent 772	4
A350-900	66.80	64.75	Trent XWB-84	3
A350-1000	73.79	64.75	Trent XWB-97	2
CRJ-700	32.48	23.25	CF34-8B	5
DHC-8-400	32.83	28.42	PW150A	2
MD-11F	61.62	51.97	CF6-80C2	1
Gulfstream V	29.39	28.50	BR700-710A	1
Cessna 525 Citation M2	12.98	14.40	FJ44	1

3   RESULTS

3.1   Beamforming results

Figure 4 shows beamforming results for the Boeing B787-8 aircraft type at emission angles of 27º, 57º, 87º, 117º, and 147º at a sound frequency of 500 Hz band. Although the drawing shows slats and flaps retracted, they were in fact fully extended for landing. The left column shows results for aircraft powered by the Engine Alliance Genx-1B70 engine, and the right column shows those for the Rolls-Royce Trent 1000 engine. At $\theta = 27º$ and 147º, sound sources appear stretched in the longitudinal direction of the aircraft due to lack of spatial resolution in that direction. The nose and main landing gears are found to be the dominant noise sources at all angles. For Trent 1000-powered aircraft, there are strong noise sources behind the engines (in this case, especially behind the left engine). In case of the Genx-1B70 engine, engine noise is slightly lower overall but stands out at an emission angle of 117º.

Figure 5 shows beamforming results for 1.6 kHz band. The nose and main landing gears are still the dominant noise sources at all emission angles, but there exist strong noise sources in front of the engines when the aircraft is moving towards the array (at emission angles of 27º and 57º). Acoustic maps outside the aircraft seem to be contaminated by sidelobes due to the poor main lobe to sidelobe ratio discussed in section 2.1.

3.2   Sound pressure level measured by the array center microphone

Figure 6 shows SPLs measured by the array center microphone at different emission angles. Time delay was considered based on Eq. (2). No corrections are applied to the raw data except for ground reflection as discussed in section 2.3 and A-weighting, so the results include a frequency shift due to Doppler effect. The left-hand graphs show all 29 data sets acquired from B787-8 flyovers. Eighteen sets of fly-over data for Genx-1B70 engines are indicated by red lines, and eleven sets of fly-over data for Trent 1000 engines are indicated by red lines. The right-hand graphs show the power-averaged spectra of each set. From the beamforming results discussed in section 3.1, the maximum SPL around 1.6 kHz must be dominated by landing gear noise. At an emission angle of 117º, the SPL of the Trent 1000-powered aircraft is larger due to the larger sound source behind engines; however, the small overall difference between the two engine types implies that airframe noise is dominant.
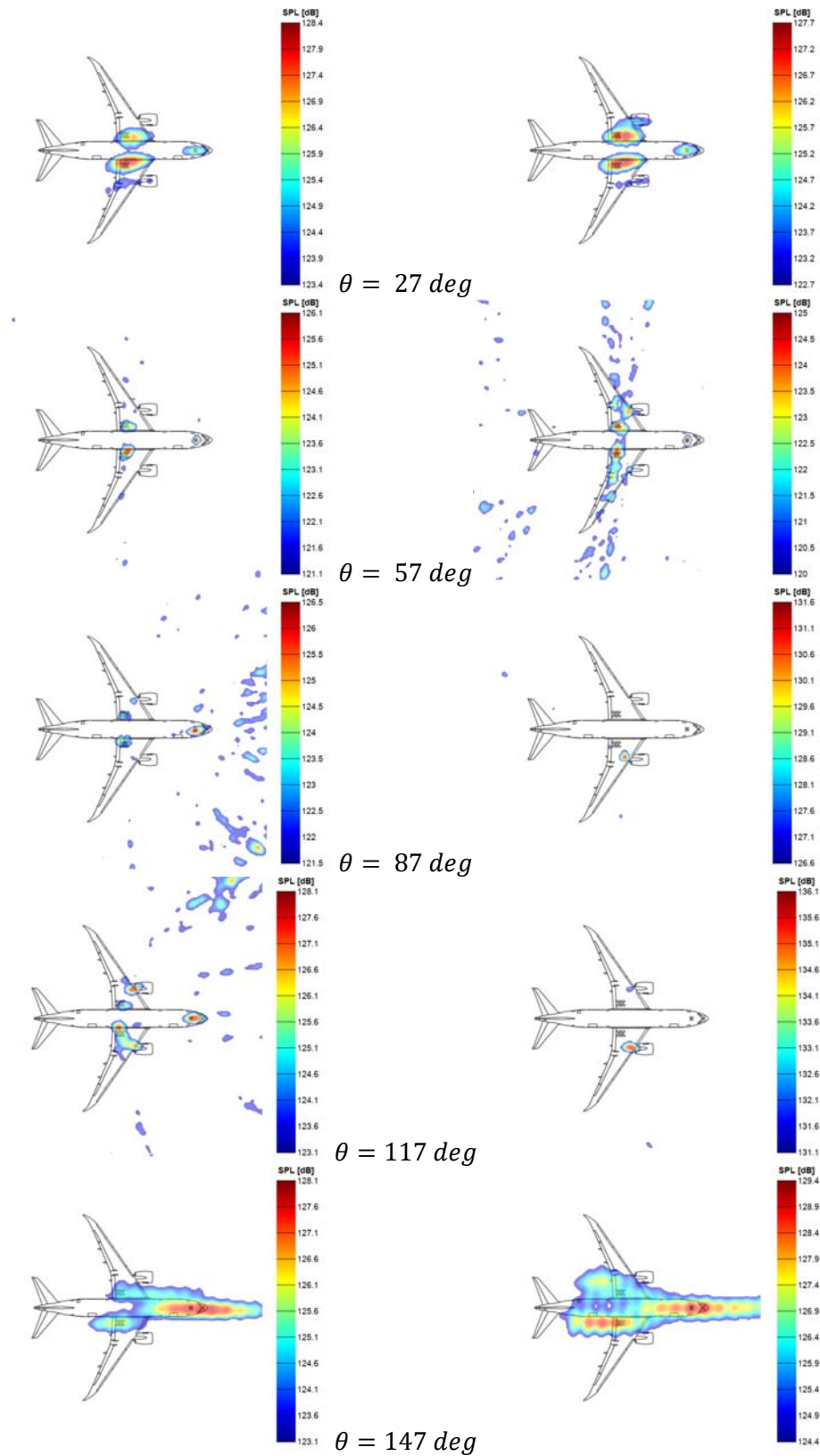
Fig.4. Beamforming results at different emission angles (500 Hz band).
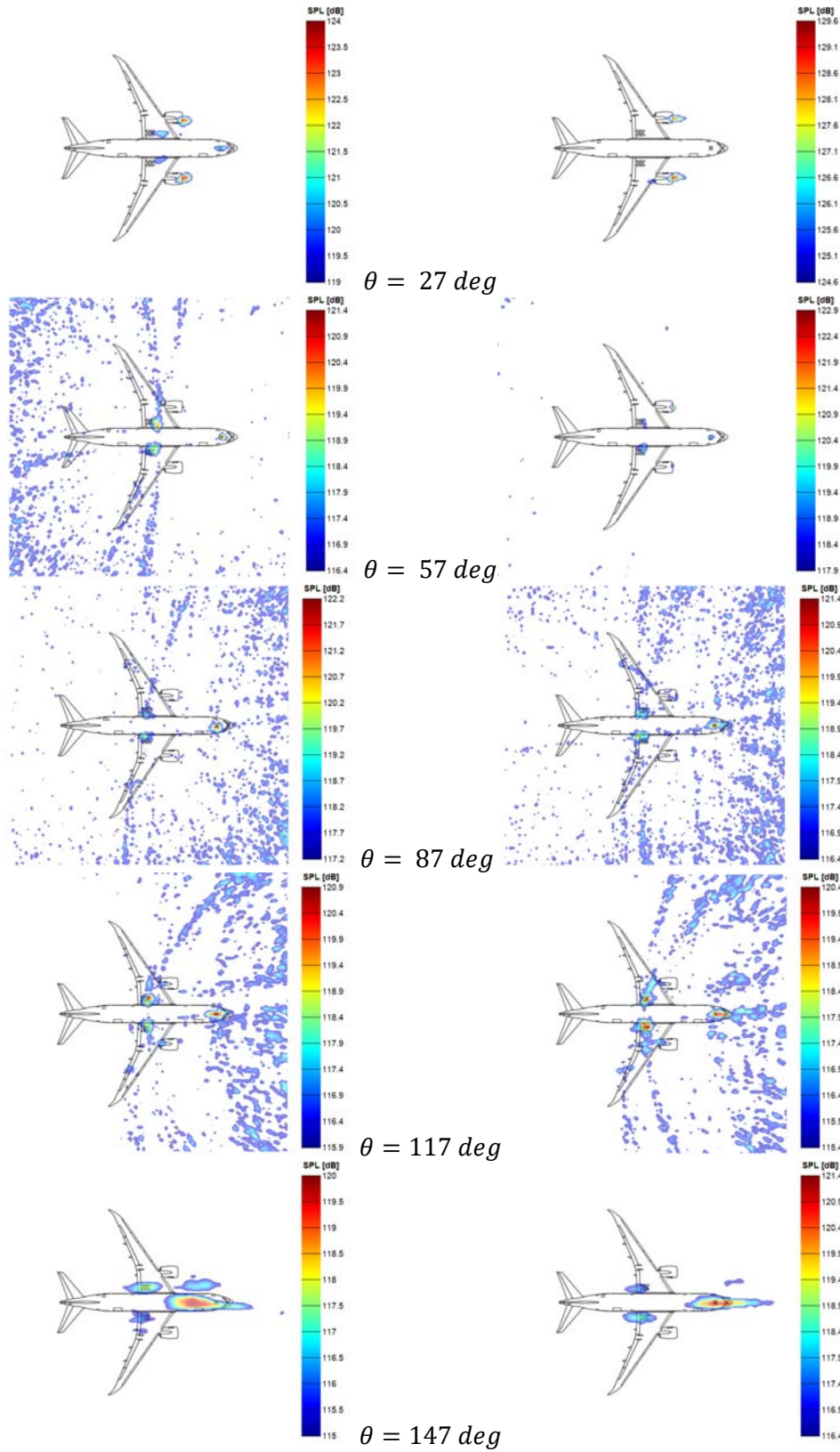*Left: B787-8 with Genx-1B70, Right: B787-8 with Trent 1000*

Fig. 5. Beamforming results at different emission angles (1.6 kHz band).
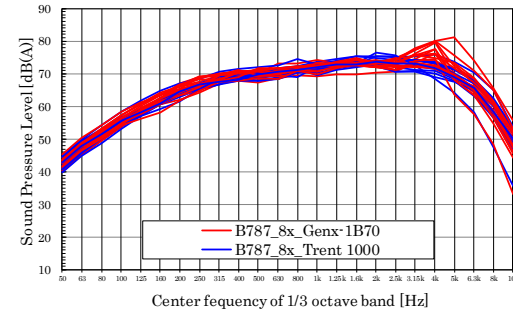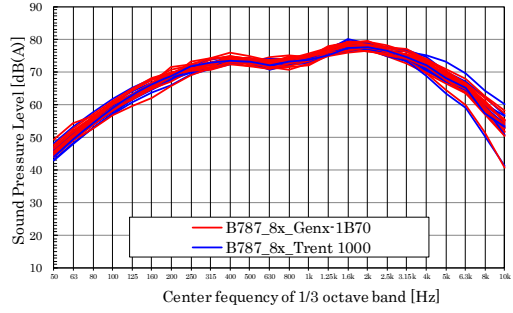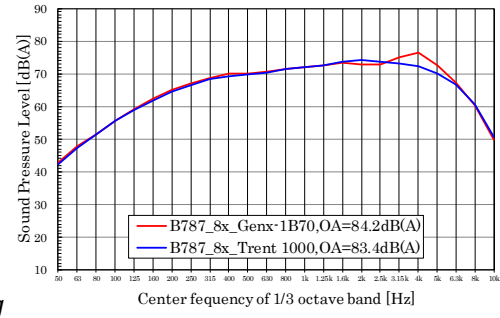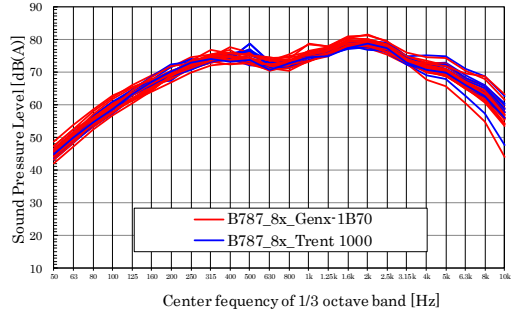*Left: B787-8 with Genx-1B70, Right: B787-8 with Trent 1000*
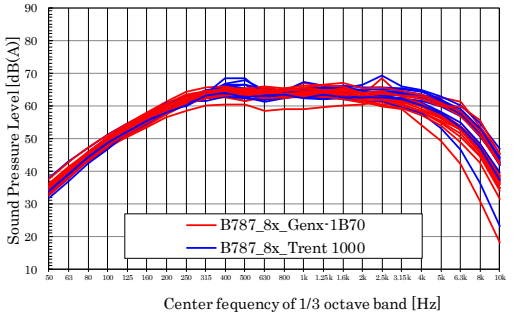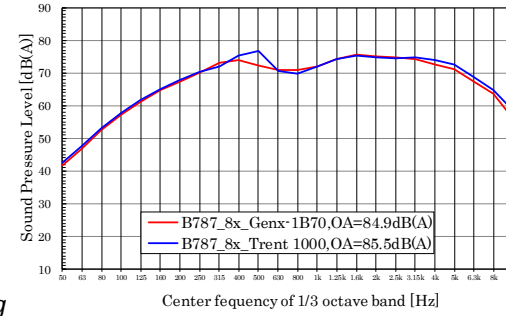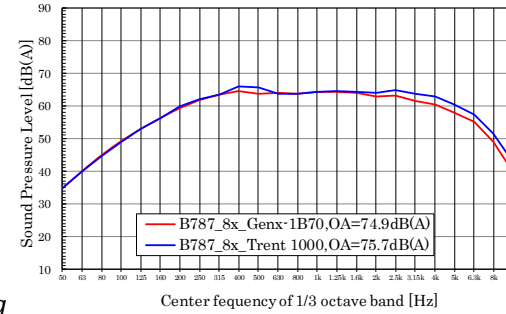
$\theta = 27\ deg$

$\theta = 57\ deg$
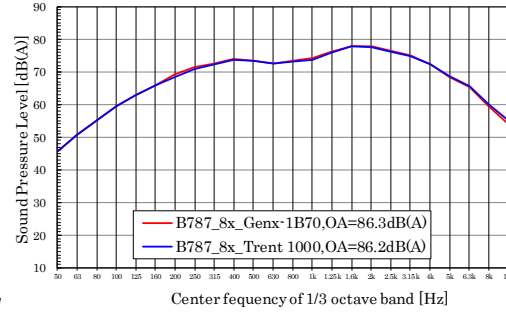
$\theta = 87\ deg$
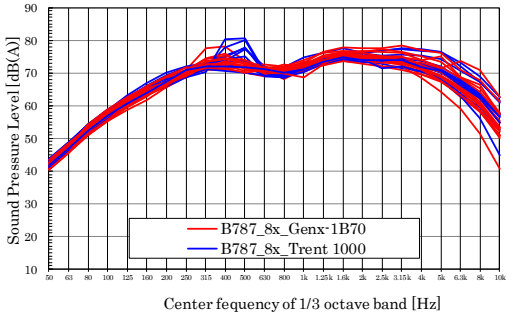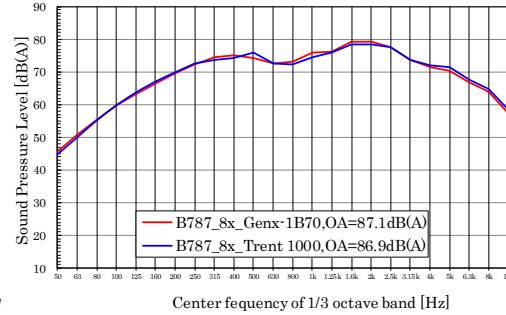
$\theta = 117\ deg$

$\theta = 147\ deg$

Fig. 6. Sound pressure level measured by the array center microphone at different emission angles.
Left: All data, Right: Power-averaged spectrum

9

3.3 Power level of each sound source (Improvement of domain integration)

Next, the power spectrum of each sound source is estimated by domain integration of the acoustical map. Figure 7 shows 13 partial regions that are defined around typical sound sources of the B787-8. Since an acoustical map can be regarded as a convolution of the true sound sources and the Point Spread Function, the integration of the acoustical map should be normalized by dividing the surface integral value of the Point Spread Function for the same region [4].
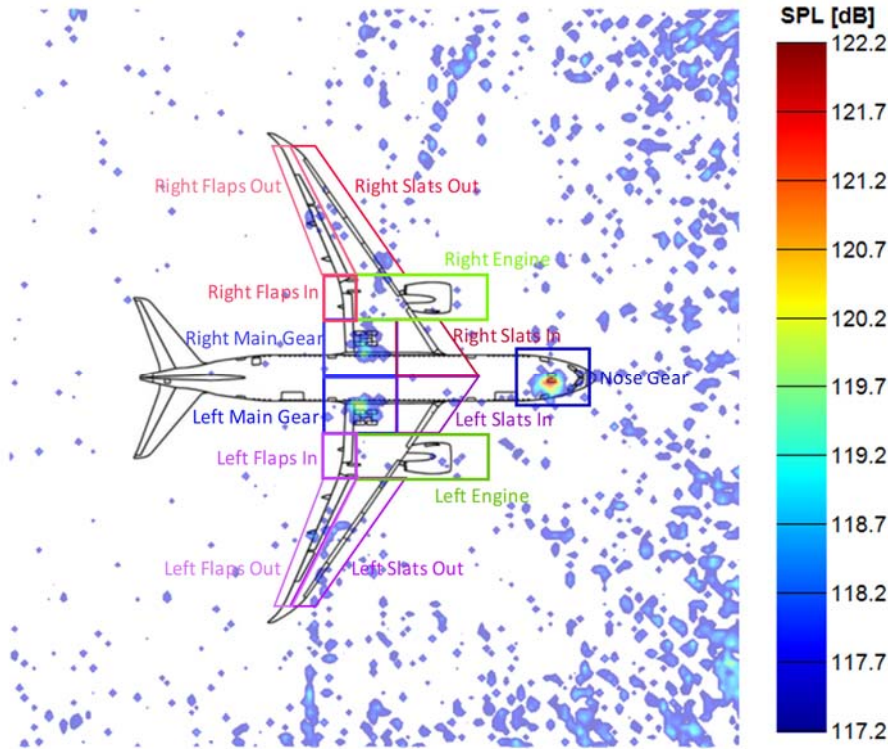
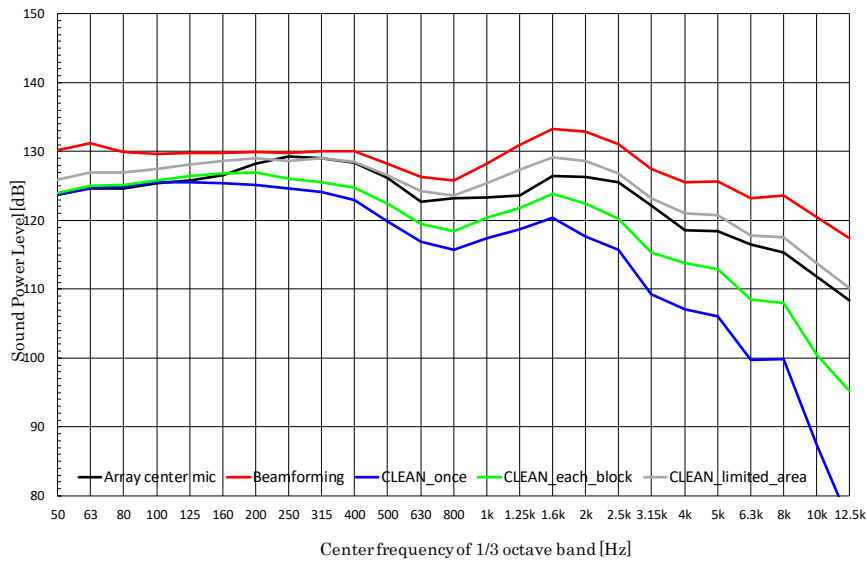*Fig. 7. Definition of 13 integration regions around B787-8.*

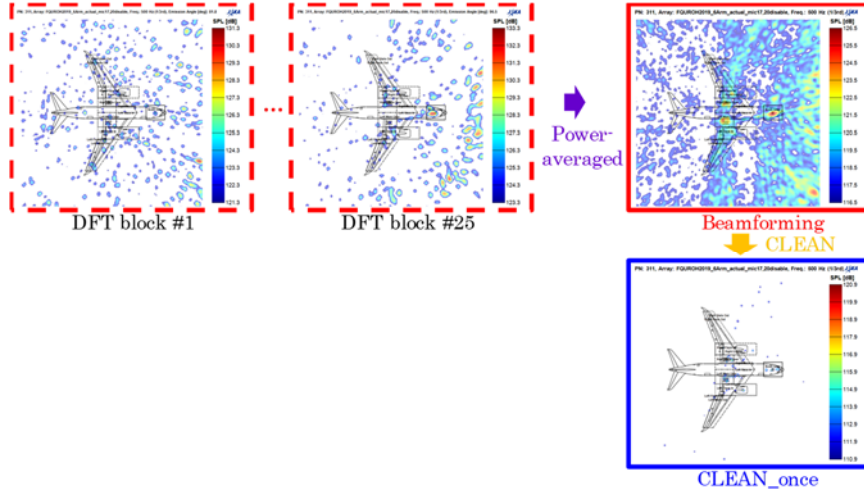*Fig. 8. Comparison of the power sum of 13 partial regions with different methods.*

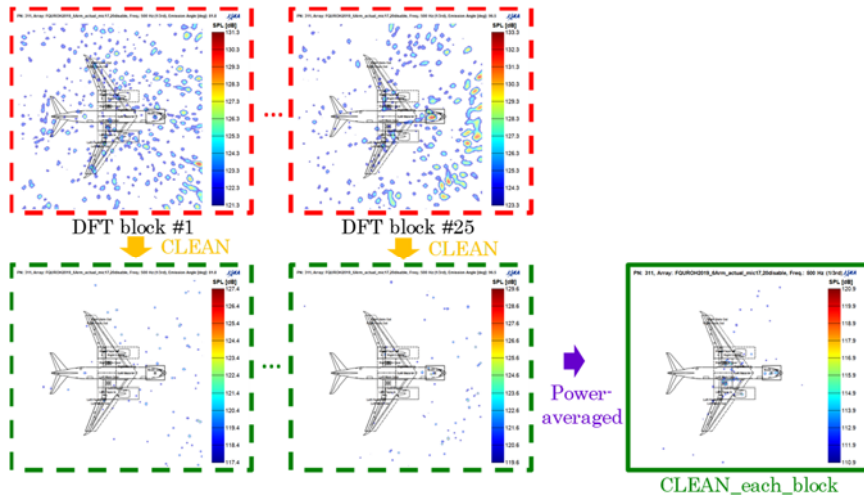*Fig. 9. CLEAN applied once to power-averaged beamforming results.*

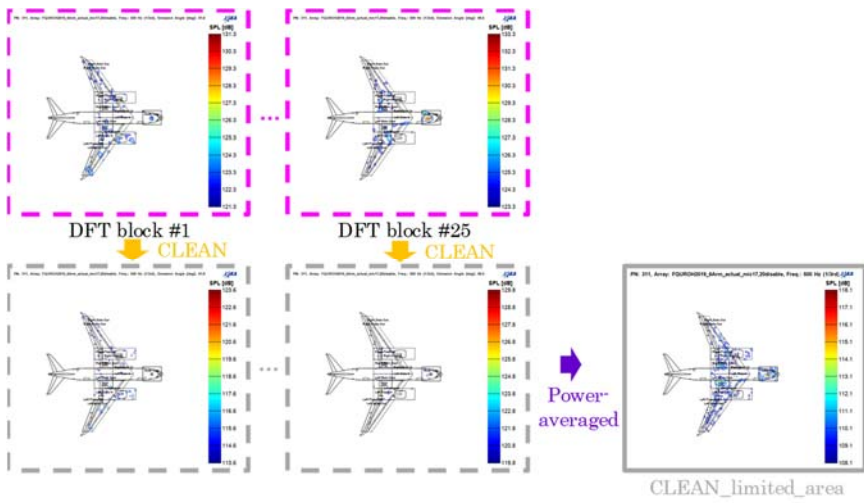*Fig. 10. CLEAN applied to beamforming result at each block.*

Fig. 11. CLEAN only applied to sound sources inside partial regions.

$\theta = 27\ deg$

$\theta = 57\ deg$

$\theta = 87\ deg$
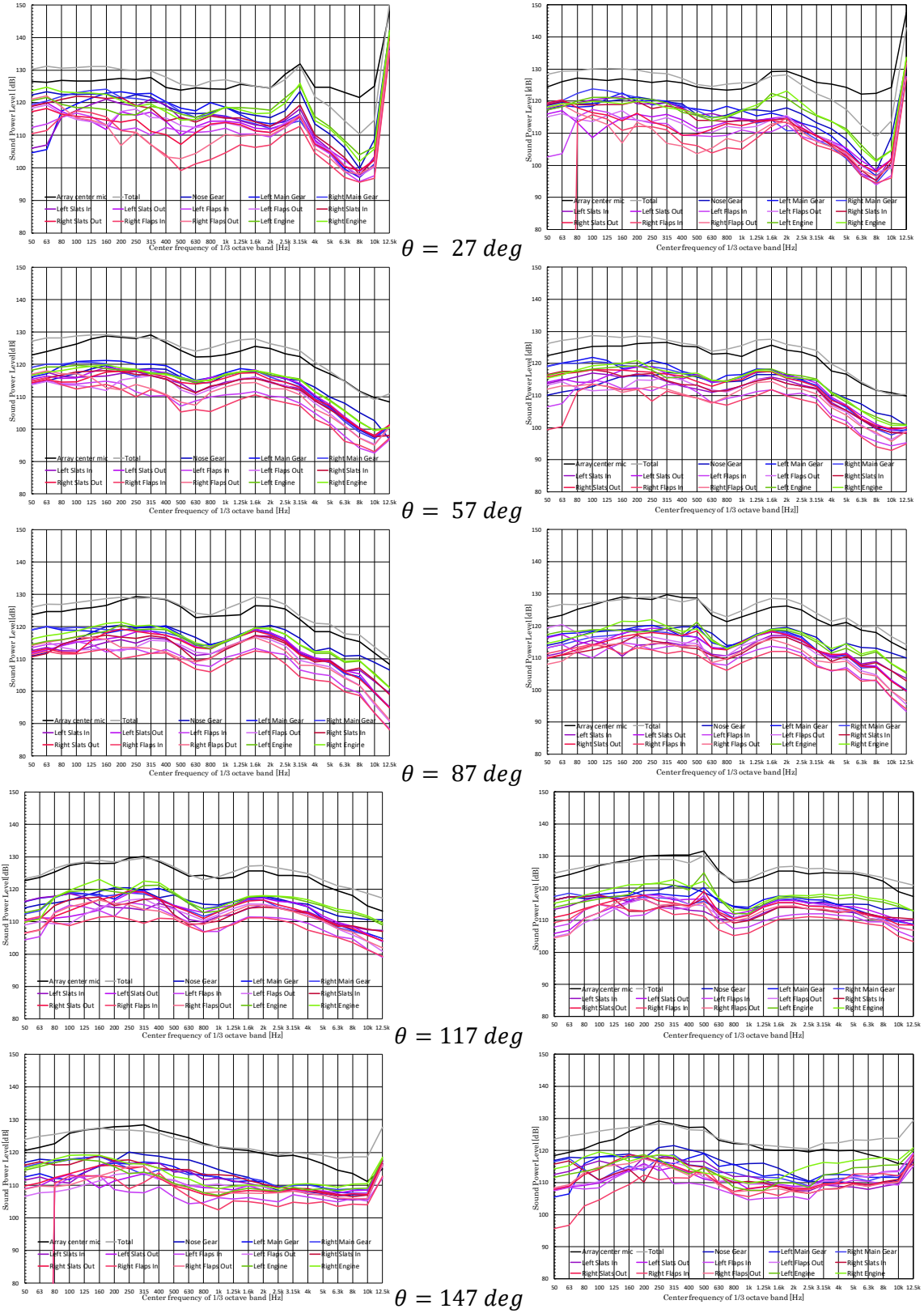
$\theta = 117\ deg$

$\theta = 147\ deg$

Fig. 12. Power levels of each sound source at different emission angles.
Left: B787-8 with Genx-1B70, Right: B787-8 with Trent 1000

Figure 8 compares the power sums of 13 partial regions computed by different methods, and Figs. 9 to 11 illustrate the calculation procedure of each method. If the power-averaged beamforming result (red solid box in Fig. 9) is integrated over 13 partial regions and summed, the sound power level (red line in Fig. 8) is larger than the level actually measured by the array center microphone (black line) due to poor resolution and sidelobes. Therefore, CLEAN [6] with the Point Spread Function computed at the mid aircraft position was applied once to the result (blue solid box in Fig. 9), but this resulted in too many powers being removed at once (blue line in Fig. 8). Then, CLEAN was applied to the beamforming result at each DFT block with the Point Spread Function computed for the actual position of the aircraft in each average and power-averaged afterwards, as illustrated in Fig. 10. This process (green line in Fig. 8) gives better prediction, but still underestimates because non-physical sources outside the aircraft are detected as sound sources, and true sound powers inside the partial regions are extracted as sidelobes of pseudo sources. Finally, sound power outside the partial regions were assumed to be 0, and CLEAN was applied only to sound sources inside the regions at each DFT block, as illustrated in Fig. 11. The resulting predicted level (gray line in Fig. 8) agrees well with the measured level. The same method was applied at the other emission angles, and Fig. 12 shows the resulting power level of each sound source.

3.4   Prediction of time histories of the sound pressure level on the ground

In order to validate the proposed sound source model, time histories of SPL on the ground were predicted by the following relations [3]

$$L_{p,i}(t + \Delta t_i(t), f_r) = L_{w,i}(\theta_i(t), f_e) - 10\log_{10}(4\pi(r_i(t)(1 - Mcos\theta_i(t)))^2) - \Delta L \tag{9}$$

$$f_e = f_r(1 - Mcos\theta_i(t)) \tag{10}$$

$$\Delta t_i(t) = r_i(t)/c \tag{11}$$

where $L_{p,i}(t, f_r)$ is the SPL of the *i*th noise source at the reception point, $L_{W,i}(\theta_i(t), f_e)$ is the sound power level of the source discussed in section 3.3, $r_i(t)$ is the distance between the noise source and the reception point, $\theta_i(t)$ is the emission angle, f_e is the frequency of emitted sound, f_r is the frequency received at the reception point, and $\Delta t_i(t)$ is the propagation time. These relations can be derived from Eqs. (1) and (2). ΔL in Eq. (9) represents air absorption as discussed in section 2.3. f_r takes the value of the center frequency of the 1/3 octave band, and f_e takes any value according to Eq. (10). θ_i also takes any value between 0º and 180º depending on the position of the aircraft. Thus, $L_{w,i}$ at θ_i and f_e is interpolated by Fig. 12, and the power level at frequency or emission angle outside the ranges in Fig. 12 take the same value as at outer boundary (0th-order extrapolation). The total SPL of all noise source contributions is then calculated by

$$L_p(t, f_r) = 10\log_{10}\sum_{i=1}^{N} 10^{L_{p,i}(t,f_r)/10} \tag{12}$$

$$L_p(t) = 10\log_{10}\sum_{f_r=50}^{10k} 10^{L_p(t,f_r)/10} \tag{13}$$
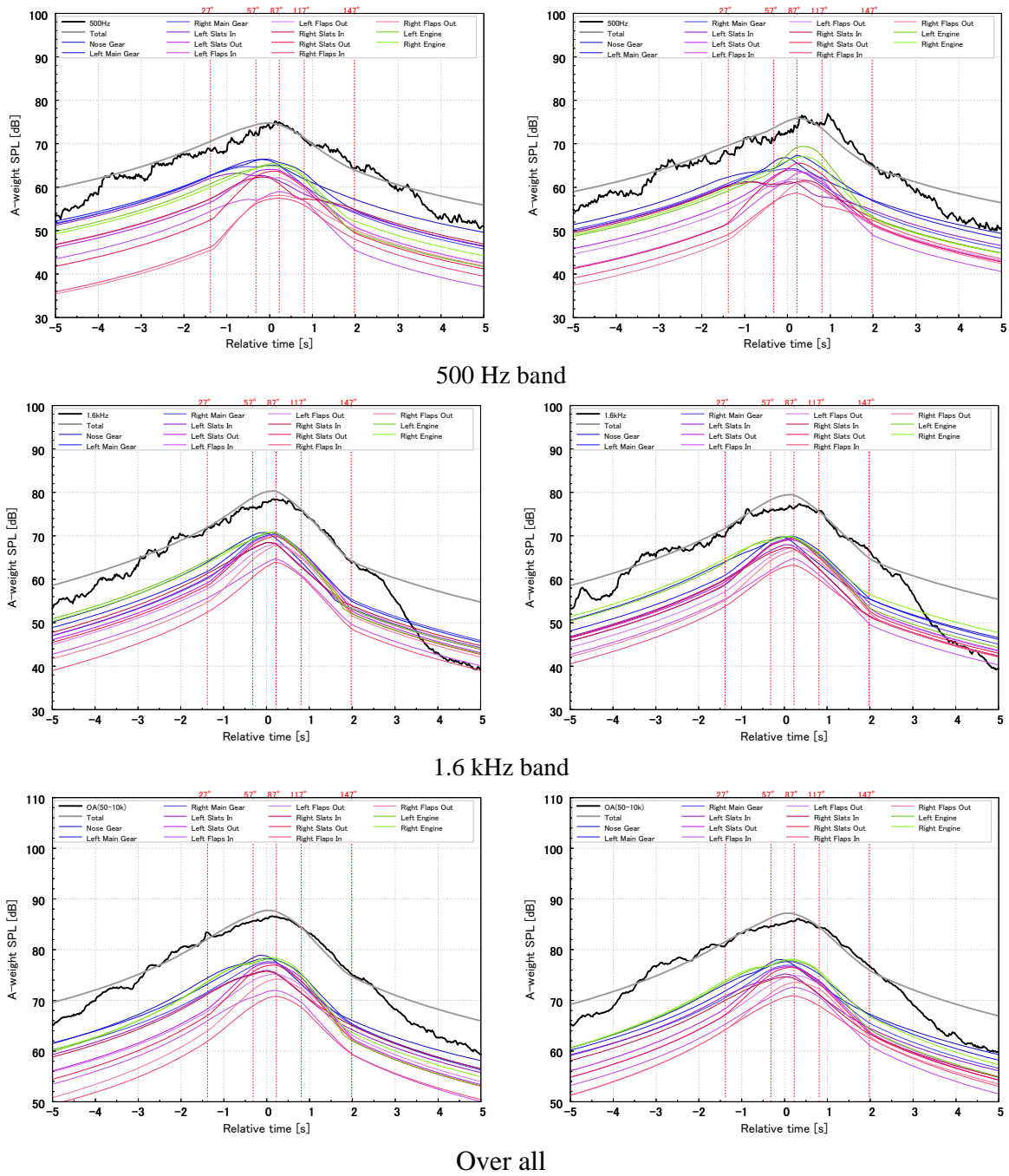
500 Hz band

1.6 kHz band

Over all

Fig. 13. Time histories of measured and predicted sound pressure levels at the array center.
Left: B787-8 with Genx-1B70, Right: B787-8 with Trent 1000

Figure 13 shows time histories of measured and predicted SPLs at the array center. The predicted total SPL (gray line) is in good agreement with the measured value (black line) at emission angles of 27º to 147º where the power level is interpolated. In the 1/3 octave band centered at 500 Hz, the nose and main landing gears are the most dominant noise sources during flyover, and the engine contribution is large at around 117º where jet noise behind the engine exit nozzle is dominant. In band around 1.6 kHz, engine noise is large in the forward

direction due to the predominance of fan noise. Landing gear noise reaches its peak level around 87°.

Finally, the single event A-weighted sound exposure level is calculated by

$$L_{AE} = 10 \log_{10} \frac{1}{T_0} \int 10^{L_p(t)/10} dt \qquad (14)$$

where T_0 is 1 s and p_0 is 20×10^{-6} Pa. Figure 14 compares the L_{AE} of the B787-8 for each engine type, and Fig. 15 shows the ratios of sound power of each major noise component. Landing gear noise is the dominant noise source, as expected from the acoustic maps. The noise contributions from slats and flaps are also large because they are distributed along the long wing spans, although their maximum levels are lower and might be contaminated by sidelobes. The influence of engine type appears to be slight, and airframe noise is responsible for 3/4 of L_{AE}.
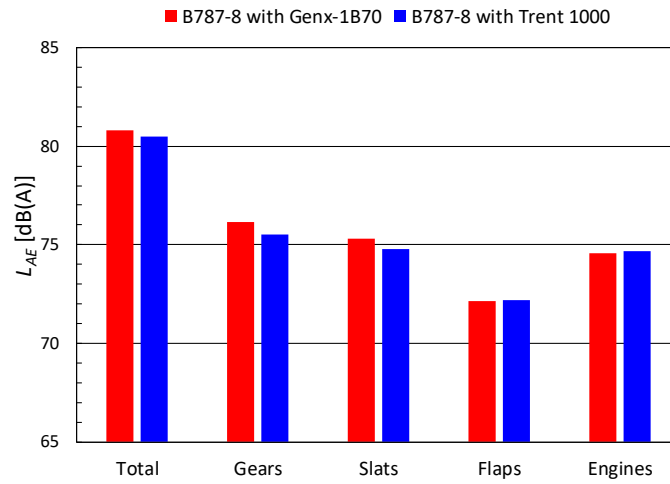

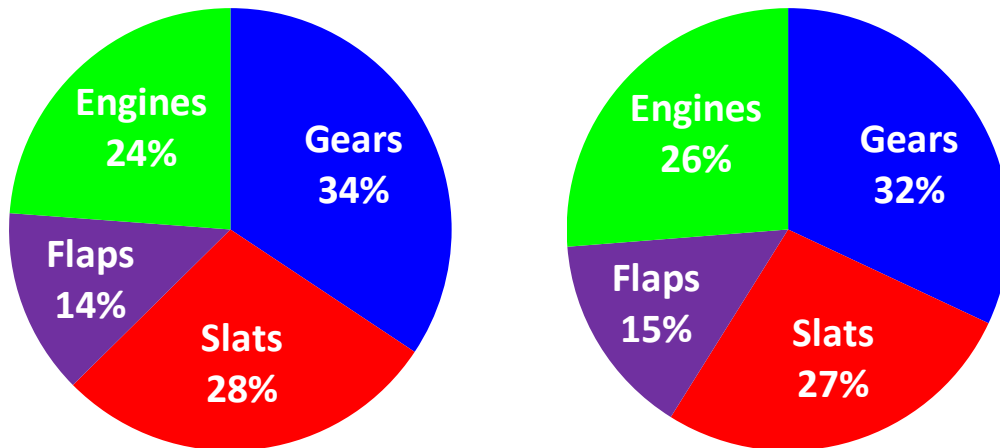Fig. 14. Comparison of L_{AE} of B787-8 with different engines.

Fig. 15. Sound power ratio for each major component.
Left: B787-8 with Genx-1B70, Right: B787-8 with Trent 1000

15

4   CONCLUSIONS

In order to model detailed sound source properties necessary for precise airport noise prediction, a 30 m-diameter microphone array of 90 microphones was deployed under the final approach path to runway 16L at Narita International Airport, and a total of 186 civil aircraft flight passes with 25 aircraft types and 33 engine types were measured over three days in May 2019. Beamforming in the time domain was applied with additional methods such as weight factors for each microphone and diagonal removal from the source power spectrum. Aircraft position tracking data were reconstructed from position and velocity directly overhead the array measured by line sensor cameras assuming flight on a 3° glideslope at a constant velocity. In case of the latest aircraft types with high-bypass turbofan engines, such as the Boeing 787, the nose and main landing gears were found to be the dominant noise sources, and seem to be the main contributors to the maximum SPL on the ground around 1.6 kHz. Acoustical maps were integrated over 13 partial regions around the aircraft to model the sound power levels and directivities of each sound source. Although the standard CLEAN algorithm removed too much of the source powers due to sidelobes, applying CLEAN to the limited regions of interest gave good estimations, and the predicted time histories of SPL on the ground agreed very well with measured values. In case of the B787-8, airframe noise was found to be responsible for 3/4 of L_{AE}. As a future problem, we are planning another flyover test with a greater number of microphones to reduce the effect of sidelobes as discussed in section 2.1.

Acknowledgements

REFERENCES

[1]   K. Yamamoto, et al. "FQUROH: A Flight Demonstration Project for Airframe Noise Reduction Technology – the 2nd Flight Demonstration." AIAA-2018-4087, 2018. 24th AIAA/CEAS Aeroacoustics Conference, Atlanta, Georgia, 25-29 June, 2018.

[2]   T. Takaishi, K. Yamamoto, T. Kobayashi, and T. Yokota. "Localization of noise sources around aircraft in flight based on time-domain beamforming technique." Proceedings of INTER-NOISE 2018, 602-613, Chicago, IL, 26-29 August, 2018.

[3]   T. Kobayashi, T. Yokota, K. Makino, and T. Takaishi. "Precise sound source model for aircraft noise prediction based on noise source distribution determined by phased array beamforming." Proceedings of INTER-NOISE 2018, 3599-3610, Chicago, IL, 26-29 August, 2018.

[4]   P. Sijtsma and R. W. Stoker. "Determination of Absolute Contributions of Aircraft Noise Components Using Fly-over Array Measurements." AIAA-2004-2958, 2004. 10th AIAA/CEAS Aeroacoustics Conference, Manchester, United Kingdom, 10-12 May, 2004.

[5]   G. P. Howell, A. J. Bradley, M. A. McCormick, and J. D. Brown. "De-Dopplerization and Acoustic Imaging of Aircraft Flyover Noise Measurements." J. Sound Vib., 105, 151–1177, 1986.

[6]   P. Sijtsma. "CLEAN Based on Spatial Source Coherence." AIAA-2007-3436, 2007. 13th AIAA/CEAS Aeroacoustics Conference, Rome, Italy, 21-23 May, 2007.